



Distinguishing intrahepatic mass-forming biliary carcinomas from hepatocellular carcinoma by computed tomography and magnetic resonance imaging using the Bayesian method: A bi-center study

メタデータ	言語: English 出版者: Springer Nature 公開日: 2025-06-27 キーワード (Ja): キーワード (En): intrahepatic cholangiocarcinoma, hepatocellular carcinoma, multidetector computed tomography, magnetic resonance imaging, Bayesian method 作成者: Ichikawa, Shintaro, Isoda, Hiroyoshi, Shimizu, Tatsuya, Tamada, Daiki, Taura, Kojiro, Togashi, Kaori, Onishi, Hiroshi, Motosugi, Utaroh メールアドレス: 所属:
URL	http://hdl.handle.net/10271/0002000459

Distinguishing intrahepatic mass-forming biliary carcinomas from hepatocellular carcinoma by computed tomography and magnetic resonance imaging using the Bayesian method: A bi-center study

Abstract

Objectives: To determine imaging hallmarks for distinguishing intrahepatic mass-forming biliary carcinomas (IMBCs) from hepatocellular carcinoma (HCC) and to validate their diagnostic ability using Bayesian statistics.

Methods: Study 1 retrospectively identified clinical and imaging hallmarks that distinguish IMBCs ($n=41$) from HCC ($n=247$) using computed tomography (CT) and magnetic resonance imaging (MRI). Study 2 retrospectively assessed the diagnostic ability of these hallmarks to distinguish IMBCs ($n=37$) from HCC ($n=111$) using Bayesian statistics with images obtained from a different institution. We also assessed the diagnostic ability of the hallmarks in the patient subgroup with high diagnostic confidence ($\geq 80\%$ of post-test probability). Two radiologists independently evaluated the imaging findings in Study 1 and 2.

Results: In Study 1, arterial phase peri-tumoral parenchymal enhancement on CT/MRI, delayed enhancement on CT/MRI, diffusion-weighted imaging peripheral hyperintensity, and bile duct dilatation were hallmarks indicating IMBCs, whereas chronic liver disease, non-rim arterial phase hyperenhancement on CT/MRI, enhancing capsule on CT/MRI, and opposed-phase signal drop were hallmarks indicating HCC ($P=0.001-0.04$). In Study 2, Bayesian statistics-based post-test probability combining all hallmark features had a diagnostic accuracy of 89.2% (132/148) in distinguishing IMBCs from HCC for both readers. In the high diagnostic confidence subgroup ($n=120$ and $n=124$ for reader 1 and 2, respectively), the accuracy improved (95.0% (114/120) and 93.5% (116/124) for reader 1 and 2, respectively).

Conclusions: Combined interpretation of CT and MRI to identify hallmark features is useful in discriminating IMBCs from HCCs. High post-test probability by Bayesian statistics allows for a more reliable non-invasive diagnosis.

Keywords

intrahepatic cholangiocarcinoma; hepatocellular carcinoma; multidetector computed tomography; magnetic resonance imaging; Bayesian method

Key Points

- Combined interpretation of CT and MRI to identify hallmark features was useful in discriminating intrahepatic mass-forming biliary carcinomas from hepatocellular carcinoma.
- Bayesian method-based post-test probability combining all hallmark features determined in Study 1 showed high (>90%) sensitivity and specificity for distinguishing intrahepatic mass-forming biliary carcinomas from hepatocellular carcinoma.
- If the post-test probability or the confidence was $\geq 80\%$ when combining the imaging features of CT and MRI, the high specificity of >95% was achieved without any loss of sensitivity to distinguish hepatocellular carcinoma from intrahepatic mass-forming biliary carcinomas.

List of abbreviations

IMBC, intrahepatic mass-forming biliary carcinoma; HCC, hepatocellular carcinoma; MRI, magnetic resonance imaging; CT, computed tomography; T1WI, T1-weighted image; T2WI, T2-weighted image; DWI, diffusion-weighted image; APHE, arterial phase hyperenhancement; PVP, portal venous phase; HBP, hepatobiliary phase

Introduction

Chronic liver disease (CLD) is a well-known risk factor for hepatocellular carcinoma (HCC) and intrahepatic cholangiocarcinoma (ICC) [1, 2]. Cholangiolocellular carcinoma (CoCC) and combined hepatocellular-cholangiocarcinoma (cHCC-CC) are rare primary liver tumors that were once considered to be distinct subtypes of ICC [3, 4] but have recently been classified as two distinctive entities [5]. CoCC and cHCC-CC still share demographic and clinical similarities with ICC and risk factors with HCC [6, 7], and are collectively referred to as intrahepatic mass-forming biliary carcinomas (IMBCs). IMBCs are the second most common type of liver tumors after HCC and their worldwide incidence is increasing [2]. HCC features have been well described using computed tomography (CT) and magnetic resonance imaging (MRI), and these descriptions have helped establish an HCC diagnosis algorithm (Liver Reporting and Data System (LI-RADS) [8]. In the LI-RADS criteria, specificity is an important benchmark for the LR-5 category, where an HCC diagnosis is confirmed without a biopsy. However, sensitivity for LR-5 is relatively low, at around 70–80% [9, 10].

Gadoxetate disodium is a liver-specific contrast agent that allows for both dynamic study and liver-specific hepatocyte imaging (hepatobiliary phase (HBP)). Gadoxetate disodium is widely used for clinical liver MRI due to its high success in lesion detection and characterization [11-13]. High lesion-to-liver contrast in HBP images offers superior sensitivity for small hepatocellular nodules including the HCCs [14-16]. However, relatively lower specificity is a concern when using gadoxetate disodium for diagnosing HCC as most intrahepatic lesions show hypointensity in HBP [17-19]. For example, since hemangioma exhibit hyperenhancement in the arterial phase and hypointensity in HBP, they can be misdiagnosed as HCCs.

Prognosis and treatment options differ significantly between IMBCs and HCC [8, 20], however, distinguishing them remains a challenge as IMBCs often present with an atypical arterial phase hyperenhancement (APHE) pattern, especially in patients with a history of

chronic liver disease or liver cirrhosis [21, 22]. Previous reports have described a combination of imaging findings for diagnosing liver lesions [23-25]. The Bayesian method, which calculates post-test probability, i.e., the most likely diagnosis and its confidence level, could be used to refine the characterization of liver lesions. Therefore, it would be possible to obtain high specificity in distinguishing IMBCs from HCC by focusing on patients that show a high post-test probability of diagnosis. The purpose of this study was to determine the hallmark features in dynamic CT and gadoteric disodium-enhanced MRI to distinguish IMBCs from HCC and to validate their diagnostic ability using the Bayesian method in separate datasets.

Materials and Methods

Study design

Study 1 retrospectively determined the hallmarks of dynamic CT and gadoteric disodium-enhanced MRI for use in Bayesian estimation to distinguish IMBCs from HCC. Study 2 retrospectively validated the diagnostic ability of those hallmarks using the Bayesian method in separate datasets (Figure 1). The trial protocol was approved by a central ethics committee and the local institutional review board. For both Studies 1 and 2, the requirement for written informed consent was waived due to the retrospective nature of the studies.

Study population

Study 1

Patients were consecutively enrolled between January 2008 and January 2016 from one hospital. The following inclusion criteria were used: i) the presence of pathologically confirmed IMBCs or HCC by resection; and ii) availability of both the dynamic CT and gadoteric disodium-enhanced MRI data within 3 months before resection. Of the 288 patients with 296 lesions enrolled in Study 1, 8 patients with 8 lesions were excluded. The final Study 1 cohort consisted of 274 patients (mean age, 70.0 ± 8.9 [range, 35–89] years) with 288 liver lesions

(Figure 1), which included 211 men (69.2 ± 8.5 [45–86] years) and 63 women (72.7 ± 9.7 [35–89] years).

Study 2

Patients were consecutively enrolled between December 2008 and March 2015 from a hospital different from Study 1 but using the same inclusion criteria as in Study 1. Of the 300 patients with 307 lesions, age and size-matched cases were established between IMBCs and HCCs at a ratio of 1:3 as the lesion size usually affects imaging features, e.g. large tumor tends to present with necrosis/hemorrhage. This ratio was set to reflect the incidence rates of ICC and HCC in the United States [2]. Age was grouped into 6 categories (30–40 years, 40–50 years, 50–60 years, 60–70 years, 70–80 years, 80–90 years,) and size was grouped into 3 categories (<3 cm, 3–5 cm, and >5 cm) for the selection. During the selection, a smaller study number had a priority over a study with larger numbers. The final Study 2 cohort consisted of 147 patients (mean age, 66.2 ± 10.0 [range, 31–86] years) with 148 liver lesions (Figure 1), including 106 men (65.9 ± 9.1 [45–86] years) and 41 women (66.9 ± 12.0 [31–83] years).

MRI and CT protocols

Gadoxetic disodium-enhanced MRI was performed using a superconducting magnet scanner operated at 1.5T or 3T. CT was performed with 64–320-detector-row CT units. Detailed MRI/CT parameters varied depending on the clinical protocol at each hospital (Supplemental Material 1 and 2).

Image analysis

All data including MRI/CT images, clinical information, and pathological records were independently collected for all patients in Study 1 and 2 by a board-certificated radiologist ([anonymized] with 11 years of experience in abdominal radiology and [anonymized] with 29

years of experience in abdominal radiology). Gadoteric disodium-enhanced MRI and dynamic CT were independently and randomly assessed by two board-certificated radiologists ([anonymized] with 11 and 5 years of experience in MRI and CT liver imaging for Study 1, and [anonymized] with 18 and 11 years of experience in MRI and CT liver imaging for Study 2, respectively). The two radiologists were aware that the patients had liver lesions but were blinded to previous imaging findings or the final diagnosis. Imaging findings that have been reported to be advantageous for an IMBCs diagnosis [23-28] or included in the LI-RADS major features including LR-M (probably or definitely malignant, not necessarily HCC) criteria, and ancillary features favoring malignancy [8], were evaluated as either present or absent. The following findings were evaluated: irregular shape, non-rim APHE on CT/MRI, AP peritumoral parenchymal enhancement on CT/MRI, enhancing capsule on CT/MRI, non-peripheral washout on CT/MRI, delayed enhancement on CT/MRI, HBP peritumoral parenchymal hypointensity, HBP hypointensity in whole, DWI peripheral hyperintensity, T2WI peripheral hyperintensity, fat-saturated T1WI hyperintensity, bile duct dilatation, and opposed-phase signal drop. Any discrepancies between the two readers in Study 1 were resolved by reaching a consensus between them after a discussion and the consensus data were used for analysis. Original data from the independent review were used to calculate interobserver agreement in Study 1. Study 2 did not require a consensus review as both reader's individual data has been reported.

Statistical analysis

In Study 1, univariate and multivariate analyses were performed to identify imaging and clinical hallmarks including age, sex, body weight, chronic liver disease, tumor markers (alpha-fetoprotein [AFP] and protein induced by vitamin K absence-II [PIVKA- II]) distinguishing IMBCs from HCC. For the univariate analysis, categorical variables were compared using the chi-squared test, whereas continuous variables were compared using the Wilcoxon test between

IMBCs and HCC. For the multivariate analysis, the odds ratio was estimated by logistic regression analysis using variables that exhibited P -values < 0.10 in the univariate analysis. Subsequently, the Bayesian method-based post-test probability was calculated in Study 2 to determine the diagnostic ability of the identified hallmarks (Supplemental material 3). A probability of more than 50% for IMBCs or HCC was considered as a positive result. The disease discriminative ability of the hallmarks combined was assessed using the receiver operating characteristic curve analysis. Accuracy, sensitivity, specificity, and the area under the curve (AUC) were calculated to differentiate the IMBCs and HCC. The discriminative ability of the Bayesian method was also calculated in the subgroup of patients who had a high post-test probability ($\geq 80\%$). LI-RADS category was also assessed for each nodule based on CT or MRI findings. Cohen's kappa values were calculated to assess interobserver agreement in both the studies. Agreement was considered as excellent for kappa values (κ) > 0.8 , good for $0.6 < \kappa \leq 0.8$, moderate for $0.4 < \kappa \leq 0.6$, fair for $0.2 < \kappa \leq 0.4$, and poor for $\kappa \leq 0.2$ [29]. All statistical analyses were performed using JMP software (version 14.1.0; SAS Institute Inc.) and MATLAB Statistics and Machine Learning Toolbox (The MathWorks, Inc.). P values < 0.05 were considered statistically significant.

Results

Study 1

Lesion characteristics

The final diagnosis for 288 liver lesions was as follows: HCC, $n = 247$ (mean size, 28.5 ± 20.6 [range, 6–167] mm); IMBCs, $n = 41$ (ICC, $n = 30$; CoCC, $n = 8$; cHCC-CC, $n = 3$) (28.3 ± 16.0 [9–87] mm) (Figure 1).

Univariate analysis and interobserver agreement

A significant difference was observed between IMBCs and HCC in regards to the presence of chronic liver disease, irregular shape, non-rim APHE on CT/MRI, AP peri-tumoral parenchymal enhancement on CT/MRI, enhancing capsule on CT or MRI, non-peripheral washout on CT/MRI, delayed enhancement on CT/MRI, HBP peritumoral parenchymal hypointensity, DWI peripheral hyperintensity, fat-saturated T1WI hyperintensity, bile duct dilatation, opposed-phase signal drop, AFP, and PIVKA- II ($P < 0.001-0.01$). Age exhibited a P -value < 0.10 (Table 1). Interobserver agreement on all items was good to excellent ($\kappa = 0.678-0.907$) (Table 1).

Multivariate analysis

Multivariate analysis revealed that AP peri-tumoral parenchymal enhancement on CT or MRI, delayed enhancement on CT/MRI, DWI peripheral hyperintensity, and bile duct dilatation favored the diagnosis of IMBCs over HCC ($P = 0.001-0.03$). In contrast, chronic liver disease, non-rim APHE on CT/MRI, enhancing capsule on CT/MRI, and opposed-phase signal drop favored the diagnosis of HCC over IMBCs ($P = 0.003-0.04$) (Table 2).

Study 2

Lesion characteristics

The final diagnosis for 148 liver lesions was as follows; HCC, $n = 111$ (mean size, 45.3 ± 31.3 [range, 8–187] mm); IMBCs, $n = 37$ (ICC, $n = 29$; CoCC, $n = 4$; and cHCC-CC, $n = 4$) (46.1 ± 28.0 [8–119] mm) (Figure 1).

Bayesian method

Bayesian method-based post-test probability combining all hallmark features determined in Study 1, exhibited high (>90%) sensitivity with reader 1 and high specificity with reader 2 for distinguishing IMBCs from HCC (Table 3). In total, 120 nodules were assessed by reader 1 and

124 nodules were assessed by reader 2, which the model classified as IMBCs or HCC with high confidence ($\geq 80\%$). The distribution of post-test probability for HCC and IMBCs is shown in Figure 2. In the high-confidence subgroup, accuracy and specificity were improved without any loss of sensitivity (Table 3).

Case examples are shown in Figures 3–6. Figures 3 and 4 present the hypervascular IMBCs cases. While the nodule in Figure 3 was categorized as LR-4 (probably HCC), the Bayesian method-based post-test probability showed high confidence for IMBCs. The nodule in Figure 4 was categorized as LR-5 (definitely HCC), however, the Bayesian method-based post-test probability did not show high confidence for HCC, and cHCC-CC was subsequently diagnosed by resection. Figure 5 presents an atypical case of HCC. While the nodule was categorized as LR-M (probably or definitely malignant, not necessarily HCC), the Bayesian method-based post-test probability did not show a high probability of IMBCs (47%), and HCC was subsequently diagnosed by resection. Figure 6 is an example where diagnosis confidence was increased by using the Bayesian method. The nodule in Figure 6 was categorized as LR-3 (intermediate probability of malignancy), however, the Bayesian method-based post-test probability exhibited a high probability of HCC.

Reproducibility of CT and MRI findings between the readers

Interobserver agreement of all items was good to excellent ($\kappa = 0.687\text{--}0.963$). Detailed results of CT/MRI findings and the LI-RADS category on CT or MRI are shown in Table 4.

Discussion

Our study revealed useful CT and MRI findings for diagnosing IMBCs including AP peritumoral parenchymal enhancement on CT/MRI, delayed enhancement on CT/MRI, DWI peripheral hyperintensity, and bile duct dilatation. In contrast, chronic liver disease, non-rim APHE on CT/MRI, enhancing capsule on CT/MRI, and opposed-phase signal drop were all the

hallmark features of HCC. These results are consistent with previous reports [23-28]. The diagnostic ability of the Bayesian method-based post-test probability for distinguishing IMBCs from HCC was good. Moreover, in the high-confidence subgroup ($\geq 80\%$), a very high specificity ($>95\%$) was achieved without any loss of sensitivity.

IMBCs are characterized by abundant fibrosis and necrosis at their center and viable tumor cells in the periphery [28, 30]. Delayed enhancement on CT/MRI is thought to be related to central fibrosis, whereas DWI peripheral hyperintensity is probably due to peripheral cellular-rich areas. IMBCs originate from the epithelial lining of the intrahepatic bile duct, so IMBCs can occlude intrahepatic bile duct and cause peripheral bile duct dilatation and cholangitis. AP peritumoral parenchymal hyperenhancement on CT or MRI may reflect such cholangitis. IMBCs can exhibit various imaging findings due to the amount of fibrotic and cellular components. In Study 1, 34.1% (14/41) of IMBCs exhibited a non-rim enhancement on CT/MRI. Of these, 35.7% (5/14) exhibited a non-peripheral washout on CT/MRI, thus resembling HCCs. Although many sequences are acquired in gadoteric disodium-enhanced MRI, only the dynamic phases can be used as major features in LI-RADS criteria [8]. In this study, we revealed that other MRI findings such as DWI peripheral hyperintensity, opposed-phase signal drop, and bile duct dilatation can be useful for distinguishing IMBCs from HCC. By combining these findings, very high specificity ($>95\%$) was achieved without any loss of sensitivity.

An advantage of the Bayesian method is that it provides a probability of diagnosis, rather than a strict yes or no decision. In a clinical setting, we routinely consider probabilities when making a decision based on the test results. We may request additional tests if the probability is too low to increase our confidence in finalizing a diagnosis. By using the Bayesian method, we can separate cases that can be confidently diagnosed from those with an uncertain diagnosis, thus avoiding unnecessary further testing.

Our results can be applied to incorporate the LI-RADS criteria. Ancillary features in LI-RADS are not currently used to upgrade LR-4 to LR-5. However, an appropriate

combination of imaging features from CT and MRI can result in a >95% specificity to distinguish HCCs from IMBCs. By applying the Bayesian approach to the definition of the LR-5 category and together with the LI-RADS table, we may be able to increase the sensitivity of LR-5 for the diagnosis of HCCs.

Our study has several limitations. First, this was a retrospective case-control study and may be subject to a selection bias. Second, in our study population, the ratio between IMBCs and HCC was different from the actual cases (IMBCs:HCC = 1:4 in Study 1 and 1:3 in Study 2). According to registry data in the Liver Cancer Study Group of Japan in 2006–2007, the ratio of ICC versus HCC was 208:15250 (\approx 1:73) in patients with chronic liver disease [31]. Therefore, in our study, the distribution of HCC and IMBCs did not represent the natural population of the country. Third, we evaluated imaging findings in patients with a relatively good liver function who were capable of undergoing surgery rather than in patients with advanced or end-stage cirrhosis and HCC. This may potentially have influenced the results.

In summary, the combined interpretation of gadoteric disodium-enhanced MRI and dynamic CT to identify hallmarks was useful in discriminating IMBCs from HCCs. The diagnostic ability of the Bayesian method-based post-test probability for distinguishing IMBCs from HCC was good, and the high post-test probability by the Bayesian method allowed for a more reliable non-invasive diagnosis.

Reference

1. Chinchilla-López P, Aguilar-Olivos NE, García-Gómez J, et al (2017) Prevalence, risk factors, and survival of patients with intrahepatic cholangiocarcinoma. *Ann Hepatol* 16:565-568
2. Massarweh NN, El-Serag HB (2017) Epidemiology of hepatocellular carcinoma and intrahepatic cholangiocarcinoma. *Cancer Control* 24:1073274817729245
3. Nakanuma Y, Kakuda Y (2015) Pathologic classification of cholangiocarcinoma: New concepts. *Best Pract Res Clin Gastroenterol* 29:277-293

4. Aishima S, Oda Y (2015) Pathogenesis and classification of intrahepatic cholangiocarcinoma: different characters of perihilar large duct type versus peripheral small duct type. *J Hepatobiliary Pancreat Sci* 22:94-100
5. Nagtegaal ID, Odze RD, Klimstra D, et al (2020) The 2019 WHO classification of tumours of the digestive system. *Histopathology* 76:182-188
6. Ariizumi S, Yamamoto M (2015) Intrahepatic cholangiocarcinoma and cholangiolocellular carcinoma in cirrhosis and chronic viral hepatitis. *Surgery Today* 45:682-687
7. Gera S, Ettl M, Acosta-Gonzalez G, Xu R (2017) Clinical features, histology, and histogenesis of combined hepatocellular-cholangiocarcinoma. *World J Hepatol* 9:300-309
8. Marrero JA, Kulik LM, Sirlin CB, et al (2018) Diagnosis, staging, and management of hepatocellular carcinoma: 2018 practice guidance by the American Association for the Study of Liver Diseases. *Hepatology* 68:723-750
9. Lee SM, Lee JM, Ahn SJ, Kang HJ, Yang HK, Yoon JH (2019) LI-RADS Version 2017 versus Version 2018: Diagnosis of hepatocellular carcinoma on gadoxetate disodium-enhanced MRI. *Radiology* 292:655-663
10. Esposito A, Buscarino V, Raciti D, et al (2020) Characterization of liver nodules in patients with chronic liver disease by MRI: performance of the Liver Imaging Reporting and Data System (LI-RADS v.2018) scale and its comparison with the Likert scale. *Radiol Med* 125:15-23
11. Chen N, Motosugi U, Morisaka H, et al (2016) Added value of a gadoxetic acid-enhanced hepatocyte-phase image to the LI-RADS System for Diagnosing Hepatocellular Carcinoma. *Magn Reson in Med Sci* 15:49-59
12. Asato N, Tsurusaki M, Sofue K, et al (2017) Comparison of gadoxetic acid-enhanced dynamic MR imaging and contrast-enhanced computed tomography for preoperative evaluation of colorectal liver metastases. *Jpn J Radiol* 35:197-205

13. Moon JY, Kim SH, Choi SY, Hwang JA, Lee JE, Lee J (2018) Differentiating malignant from benign hyperintense nodules on unenhanced T1-weighted images in patients with chronic liver disease: using gadoxetic acid-enhanced and diffusion-weighted MR imaging. *Jpn J Radiol* 36:489-499
14. Li J, Wang J, Lei L, Yuan G, He S (2019) The diagnostic performance of gadoxetic acid disodium-enhanced magnetic resonance imaging and contrast-enhanced multi-detector computed tomography in detecting hepatocellular carcinoma: A meta-analysis of eight prospective studies. *Eur Radiol* 29:6519-6528
15. Li J, Li X, Weng J, et al (2018) Gd-EOB-DTPA dynamic contrast-enhanced magnetic resonance imaging is more effective than enhanced 64-slice CT for the detection of small lesions in patients with hepatocellular carcinoma. *Medicine* 97:e13964
16. Liu X, Jiang H, Chen J, Zhou Y, Huang Z, Song B (2017) Gadoxetic acid disodium-enhanced magnetic resonance imaging outperformed multidetector computed tomography in diagnosing small hepatocellular carcinoma: A meta-analysis. *Liver Transpl* 23:1505-1518
17. Joo I, Lee JM, Lee DH, Jeon JH, Han JK (2019) Retrospective validation of a new diagnostic criterion for hepatocellular carcinoma on gadoxetic acid-enhanced MRI: can hypointensity on the hepatobiliary phase be used as an alternative to washout with the aid of ancillary features? *Eur Radiol* 29:1724-1732
18. Kim DH, Choi SH, Kim SY, Kim MJ, Lee SS, Byun JH (2019) Gadoxetic acid-enhanced MRI of hepatocellular carcinoma: Value of washout in transitional and hepatobiliary phases. *Radiology* 291:651-657
19. Vernuccio F, Cannella R, Meyer M, et al (2019) LI-RADS: Diagnostic performance of hepatobiliary phase hypointensity and major imaging features of LR-3 and LR-4 lesions measuring 10-19 mm with arterial phase hyperenhancement. *AJR Am J Roentgenol* 213:W57-W65

20. Mavros MN, Economopoulos KP, Alexiou VG, Pawlik TM (2014) Treatment and prognosis for patients with intrahepatic cholangiocarcinoma: Systematic review and meta-analysis. *JAMA Surg* 149:565-574
21. Adam SZ, Parthasarathy S, Miller FH (2015) Intrahepatic cholangiocarcinomas mimicking other lesions. *Abdom Imaging* 40:2345-2354
22. Murakami T, Tsurusaki M (2014) Hypervascular benign and malignant liver tumors that require differentiation from hepatocellular carcinoma: key points of imaging diagnosis. *Liver Cancer* 3:85-96
23. Kim R, Lee JM, Shin CI, et al (2016) Differentiation of intrahepatic mass-forming cholangiocarcinoma from hepatocellular carcinoma on gadoxetic acid-enhanced liver MR imaging. *Eur Radiol* 26:1808-1817
24. Choi SH, Lee SS, Kim SY, et al (2017) Intrahepatic cholangiocarcinoma in patients with cirrhosis: Differentiation from hepatocellular carcinoma by using gadoxetic acid-enhanced MR imaging and dynamic CT. *Radiology* 282:771-781
25. Sheng RF, Zeng MS, Rao SX, Ji Y, Chen LL (2014) MRI of small intrahepatic mass-forming cholangiocarcinoma and atypical small hepatocellular carcinoma (≤ 3 cm) with cirrhosis and chronic viral hepatitis: a comparative study. *Clin Imaging* 38:265-272
26. Kim SA, Lee JM, Lee KB, et al (2011) Intrahepatic mass-forming cholangiocarcinomas: enhancement patterns at multiphasic CT, with special emphasis on arterial enhancement pattern--correlation with clinicopathologic findings. *Radiology* 260:148-157
27. Park HJ, Kim YK, Park MJ, Lee WJ (2013) Small intrahepatic mass-forming cholangiocarcinoma: target sign on diffusion-weighted imaging for differentiation from hepatocellular carcinoma. *Abdom Imaging* 38:793-801

28. Haradome H, Unno T, Morisaka H, et al (2017) Gadoteric acid disodium-enhanced MR imaging of cholangiolocellular carcinoma of the liver: imaging characteristics and histopathological correlations. *Eur Radiol* 27:4461-4471
29. McHugh ML (2012) Interrater Reliability: The Kappa Statistic. *Biochem Med (Zagreb)* 22:276-282
30. Jeong HT, Kim MJ, Chung YE, Choi JY, Park YN, Kim KW (2013) Gadoteric acid disodium-enhanced MRI of mass-forming intrahepatic cholangiocarcinomas: Imaging-histologic correlation. *AJR Am J Roentgenol* 201:W603-W611
31. Kudo M, Izumi N, Ichida T, et al (2016) Report of the 19th follow-up survey of primary liver cancer in Japan. *Hepatol Res* 46:372-390

Table and Figure Legends

Table 1. Univariate Analysis and Interobserver Agreement of IMBCs vs. HCC in Study 1

Note.—Continuous variables were analyzed by the Wilcoxon test and are expressed as mean \pm standard deviation (age, body weight, and size) or median with 25th percentile and 75th percentile (AFP and PIVKA-II). Categorical variables were analyzed by the χ^2 test and are expressed as a percentage with numerators and denominators. Kappa values are presented with the 95% confidence interval in parentheses.

$^\dagger P < 0.10$, $*P < 0.05$

IMBCs = intrahepatic mass-forming biliary carcinoma. HCC = hepatocellular carcinoma. APHE = arterial phase hyperenhancement. CT = computed tomography. MRI = magnetic resonance imaging. AP = arterial phase. HBP = hepatobiliary phase. DWI = diffusion-weighted image. T2WI = T2-weighted image. T1WI = T1-weighted image. AFP = alpha-fetoprotein. PIVKA-II = protein induced by vitamin K absence-II.

Table 2. Multivariate Analysis for Distinguishing IMBCs from HCC

Note.—Parenthesis of odds ratios are presented 95% confidence interval.

$*P < 0.05$

IMBCs = intrahepatic mass-forming biliary carcinoma. HCC = hepatocellular carcinoma. APHE = arterial phase hyperenhancement. AFP = alpha-fetoprotein. PIVKA-II = protein induced by vitamin K absence-II. CT = computed tomography. MRI = magnetic resonance imaging. AP = arterial phase. HBP = hepatobiliary phase. DWI = diffusion-weighted image. T1WI = T1-weighted image. NA = not applicable.

Table 3. Results of Study 2 by Bayesian Method to Distinguish IMBC from HCC

Note.—AUC = area under the curve. LR+ = positive likelihood ratio. LR- = negative likelihood ratio. CI = confidence interval

Table 4. Inter-reader Agreement for the Assessment of CT and MRI Findings in Study 2

Note.—CT = computed tomography. MRI = magnetic resonance imaging. IMBCs = intrahepatic mass-forming biliary carcinoma. HCC = hepatocellular carcinoma. APHE = arterial phase hyperenhancement. DWI = diffusion-weighted image.

Categorical variables are expressed as percentages with numerators and denominators. Kappa values are presented with the 95% confidence interval in parentheses

Figure 1. Flowchart of Study Design and Patient Enrollment in Study 1 and 2

CT = computed tomography. MRI = magnetic resonance imaging. NASH = nonalcoholic steatohepatitis. PBC = primary biliary cholangitis. CLD = chronic liver disease. HCC = hepatocellular carcinoma. IMBCs = intrahepatic mass-forming biliary carcinoma. ICC = intrahepatic cholangiocarcinoma. CoCC = cholangiocellular carcinoma. cHCC-CC = combined hepatocellular-cholangiocarcinoma.

Figure 2. Distribution of Post-test Probability for HCC and IMBCs

The Bayesian method-based post-test probability for IMBCs was calculated in Study 2. Based on this value, cases were classified into following four groups: high post-test probability for HCC ($\leq 20\%$ for IMBCs), low post-test probability for HCC ($20\text{--}50\%$ for IMBCs), low post-test probability for IMBCs ($50\text{--}80\%$ for IMBCs), and high post-test probability for IMBCs ($\geq 80\%$ for IMBCs). Most of the cases are distributed in high post-test probability groups.

HCC = hepatocellular carcinoma. IMBCs = intrahepatic mass-forming biliary carcinoma.

Figure 3. A case with Intrahepatic Cholangiocarcinoma despite of LR-4

A 66-year-old woman with hepatitis B had intrahepatic cholangiocarcinoma (22 mm) at S3.

This lesion had hallmarks indicating both IMBCs (delayed enhancement on CT or MRI and DWI peripheral hyperintensity, arrows) and HCC (chronic liver disease and non-rim APHE on CT or MRI, dotted arrows) and was categorized as LR-4 (probably HCC). However, the Bayesian method-based post-test probability showed a high probability (92%) that the lesion was IMBCs.

The middle panel shows CT images and the bottom panel shows MRI images.

HCC = hepatocellular carcinoma. IMBCs = intrahepatic mass-forming biliary carcinoma. CT = computed tomography. MRI = magnetic resonance imaging. APHE = arterial phase

hyperenhancement. AP = arterial phase. DP = delayed phase. TP = transitional phase. DWI = diffusion-weighted image. T1WI = T1-weighted image. IP = in-phase. OP = opposed-phase.

Figure 4. A Case with Combined Hepatocellular-cholangiocarcinoma despite of LR-5

A 66-year-old man with hepatitis C had combined hepatocellular-cholangiocarcinoma (cHCC-CC) (28 mm) at S4. This lesion had hallmarks indicating both IMBCs (DWI peripheral hyperintensity, arrow) and HCC (chronic liver disease and non-rim APHE on CT or MRI, dotted arrows) and was categorized as LR-5 (definitely HCC). However, the Bayesian method-based post-test probability did not show high confidence for HCC (55%) and cHCC-CC was subsequently diagnosed by resection.

The middle panel shows CT images and the bottom panel shows MRI images.

HCC = hepatocellular carcinoma. IMBCs = intrahepatic mass-forming biliary carcinoma. CT = computed tomography. MRI = magnetic resonance imaging. APHE = arterial phase hyperenhancement. AP = arterial phase. DP = delayed phase. TP = transitional phase. DWI = diffusion-weighted image. T1WI = T1-weighted image. IP = in-phase. OP = opposed-phase. cHCC-CC = combined hepatocellular-cholangiocarcinoma

Figure 5. A Case with Hepatocellular Carcinoma despite of LR-M

A 52-year-old man with hepatitis C had HCC (30 mm) at S7/8. This lesion had hallmarks indicating both IMBCs (DWI peripheral hyperintensity, arrow) and HCC (chronic liver disease and enhancing capsule on CT or MRI, dotted arrow), and was categorized LR-M (probably or definitely malignant, not necessarily HCC). The Bayesian method-based post-test probability did not show a high probability that the lesion was IMBC (47%) and HCC was subsequently diagnosed by resection.

The middle panel shows CT images and the bottom panel shows MRI images.

HCC = hepatocellular carcinoma. IMBCs = intrahepatic mass-forming biliary carcinoma. CT = computed tomography. MRI = magnetic resonance imaging. APHE = arterial phase hyperenhancement. AP = arterial phase. DP = delayed phase. TP = transitional phase. DWI = diffusion-weighted image. T1WI = T1-weighted image. IP = in-phase. OP = opposed-phase.

Figure 6. A Case with Hepatocellular Carcinoma with High Confidence despite of LR-3

A 69-year-old woman with hepatitis C had HCC (8 mm) at S8. This lesion did not have hallmarks indicating IMBCs, whereas it had hallmarks indicating HCC (chronic liver disease and non-rim APHE on CT or MRI, dotted arrows). It seemed that this lesion showed hyperintensity on DWI; however, there was no surety because of the distorted image. This lesion was categorized LR-3

(intermediate probability of malignancy), but the Bayesian method-based post-test probability showed high probability (87%) that the lesion was HCC.

The middle panel shows CT images and the bottom panel shows MRI images.

HCC = hepatocellular carcinoma. IMBCs = intrahepatic mass-forming biliary carcinoma. CT = computed tomography. MRI = magnetic resonance imaging. APHE = arterial phase hyperenhancement. AP = arterial phase. DP = delayed phase. TP = transitional phase. DWI = diffusion-weighted image. T1WI = T1-weighted image. IP = in-phase. OP = opposed-phase.

Table 1. Univariate Analysis and Interobserver Agreement of IMBCs vs. HCC in Study 1

Variables	IMBCs (n=41)	HCC (n=247)	<i>P</i> value	Kappa value
Age [years]	68.1 ± 7.0	70.3 ± 9.2	0.05 [†]	-
Sex [M:F]	33:5	178:58	0.15	-
Body weight [kg]	59.6 ± 9.8	59.7 ± 10.8	0.96	-
Chronic liver disease	55.2% (21/38)	99.6% (235/236)	< 0.001*	-
AFP [nmol/L]	1.2 (0.7, 1.7)	2.4 (1.2, 7.8)	< 0.001*	-
PIVKA-II [AU/L]	18.5 (15, 26.8)	29 (19, 130.5)	0.002*	-
Size [mm]	28.3 ± 15.9	28.5 ± 20.6	0.66	-
Irregular shape	19.5% (8/41)	0% (0/247)	< 0.001*	0.815 (0.725–0.905)
Non-rim APHE on CT/MRI	34.1% (14/41)	96.8% (239/247)	< 0.001*	0.766 (0.672–0.859)
AP peri-tumoral parenchymal enhancement on CT/MRI	56.1% (23/41)	19.8% (49/247)	0.001*	0.678 (0.579–0.776)
Enhancing capsule on CT/MRI	22.0% (9/41)	82.2% (203/247)	< 0.001*	0.705 (0.618–0.792)
Non-peripheral washout on CT/MRI	39.0% (16/41)	92.3% (228/247)	< 0.001*	0.786 (0.674–0.898)
Delayed enhancement on CT/MRI	70.7% (29/41)	1.62% (4/247)	< 0.001*	0.746 (0.628–0.865)
HBP peritumoral parenchymal hypointensity	31.7% (13/41)	10.9% (27/247)	0.001*	0.692 (0.569–0.815)
HBP hypointensity in whole	87.8% (36/41)	78.1% (193/247)	0.21	0.734 (0.635–0.833)
DWI peripheral hyperintensity	26.8% (11/41)	4.45% (11/247)	< 0.001*	0.777 (0.671–0.882)

T2WI peripheral hyperintensity	19.5% (8/41)	11.7% (29/247)	0.20	0.668 (0.567–0.770)
Fat-saturated T1WI hyperintensity	9.76% (4/41)	30.4% (75/247)	0.005*	0.843 (0.773–0.913)
Bile duct dilatation	26.8% (11/41)	2.83% (7/247)	< 0.001*	0.904 (0.796–1.000)
Opposed-phase signal drop	0% (0/41)	34.4% (85/247)	< 0.001*	0.907 (0.854–0.961)

Note.—Continuous variables were analyzed by Wilcoxon test and are expressed as mean \pm standard deviation (age, body weight, and size) or median with 25th percentile and 75th percentile (AFP and PIVKA-II). Categorical variables were analyzed by the χ^2 test and are expressed as percentage with numerators and denominators. Kappa values are presented with the 95% confidence interval in parentheses.

$\dagger P < 0.10$, $*P < 0.05$

IMBCs = intrahepatic mass-forming biliary carcinoma. HCC = hepatocellular carcinoma. APHE = arterial phase hyperenhancement. CT = computed tomography. MRI = magnetic resonance imaging. AP = arterial phase. HBP = hepatobiliary phase. DWI = diffusion-weighted image. T2WI = T2-weighted image. T1WI = T1-weighted image. AFP = alpha-fetoprotein. PIVKA-II = protein induced by vitamin K absence-II.

Table 2. Multivariate Analysis for Distinguishing IMBCs from HCC

Variables	Odds ratio (IMBCs vs. HCC)	<i>P</i> value
Age	0.91 (0.81–1.02)	0.09
Chronic liver disease	0.02 (1.5×10^{-3} –0.6)	0.02*
AFP	1.0 (1.0–1.0)	0.80
PIVKA-II	1.0 (1.0–1.0)	0.88
Irregular shape	11.5 (6.2×10^{-3} – 2.2×10^4)	0.52
Non-rim APHE on CT/MRI	0.03 (2.5×10^{-3} –0.3)	0.003*
AP peri-tumoral parenchymal enhancement on CT/MRI	3.3 (1.3–8.3)	0.01*
Enhancing capsule on CT/MRI	0.1 (0.01–0.6)	0.02*
Non-peripheral washout on CT/MRI	0.2 (0.02–2.8)	0.24
Delayed enhancement on CT/MRI	96.3 (6.2–1495.3)	0.001*
HBP peritumoral parenchymal hypointensity	1.3 (0.1–17.7)	0.82
DWI peripheral hyperintensity	54.5 (2.8–1078.0)	0.01*
Fat-saturated T1WI hyperintensity	0.8 (0.1–10.9)	0.85
Bile duct dilatation	27.9 (1.4–571.2)	0.03*
Opposed-phase signal drop	0.02 (4.0×10^{-4} –0.8)	0.04*

Note.—Parenthesis of odds ratios are presented 95% confidence interval.

* $P < 0.05$

IMBCs = intrahepatic mass-forming biliary carcinoma. HCC = hepatocellular carcinoma. APHE = arterial phase hyperenhancement. AFP = alpha-fetoprotein. PIVKA-II = protein induced by vitamin K absence-II. CT = computed tomography. MRI = magnetic resonance imaging. AP = arterial phase. HBP = hepatobiliary phase. DWI = diffusion-weighted image. T1WI = T1-weighted image. NA = not applicable.

Table 3. Results of Study 2 by Bayesian Method to Distinguish IMBC from HCC

	All nodules (<i>n</i> =148)		High ($\geq 80\%$) post-test probability group	
	Reader 1	Reader 2	Reader 1 (<i>n</i> =120)	Reader 2 (<i>n</i> =124)
AUC (95% CI)	0.96 (0.90–0.99)	0.94 (0.88–0.97)	0.97 (0.91–0.99)	0.96 (0.90–0.99)
Accuracy (n/n)	89.2% (132/148)	89.2% (132/148)	95.0% (114/120)	93.5% (116/124)
Sensitivity (n/n)	91.9% (34/37)	83.8% (31/37)	93.9% (31/33)	84.8% (28/33)
Specificity (n/n)	88.3% (98/111)	91.0% (101/111)	95.4% (83/87)	96.7% (88/91)
LR+ (95% CI)	7.85 (5.32–9.72)	9.30 (5.65–14.08)	20.4 (10.2–32.5)	25.7 (10.5–68.3)
LR- (95% CI)	0.09 (0.03–0.22)	0.18 (0.09–0.32)	0.06 (0.02–0.17)	0.16 (0.10–0.28)

Note.—IMBCs = intrahepatic mass-forming biliary carcinoma. HCC = hepatocellular carcinoma. AUC = area under the curve. LR+ = positive likelihood ratio. LR- = negative likelihood ratio. CI = confidence interval

Table 4. Inter-reader Agreement for the Assessment of CT and MRI Findings in Study 2

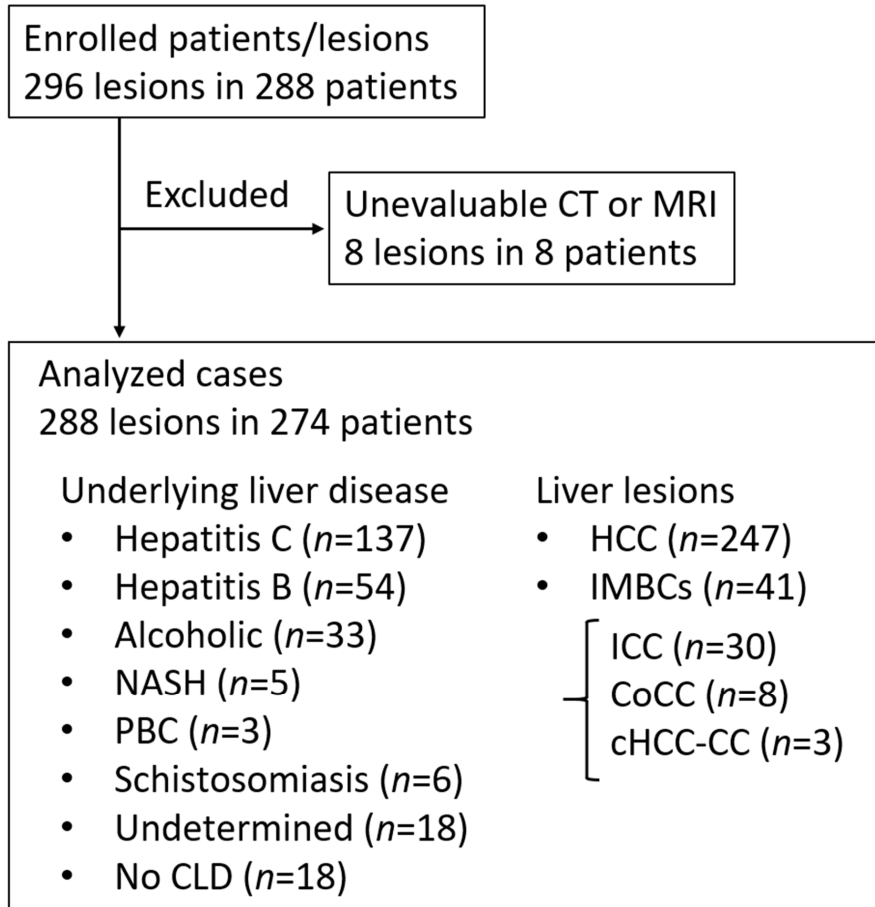
	Reader 1		Reader 2		Kappa value
	IMBCs	HCC	IMBCs	HCC	
Non-rim APHE on CT/MRI	29.7% (11/37)	91.0% (101/111)	29.7% (11/37)	93.7% (104/111)	0.830 (0.723–0.937)
AP peri-tumoral parenchymal enhancement on CT/MRI	54.1% (20/37)	18.0% (20/111)	51.4% (19/37)	17.1% (19/111)	0.687 (0.553–0.821)
Enhancing capsule on CT/MRI	18.9% (7/37)	70.2% (78/111)	13.5% (5/37)	75.7% (84/111)	0.728 (0.612–0.845)
Delayed enhancement on CT/MRI	73.0% (27/37)	4.5% (5/111)	54.0% (20/37)	2.7% (3/111)	0.800 (0.676–0.924)
DWI peripheral hyperintensity	35.1% (13/37)	8.1% (9/111)	32.4% (12/37)	7.2% (8/111)	0.723 (0.560–0.885)
Bile duct dilatation	35.1% (13/37)	5.4% (6/111)	35.1% (13/37)	6.3% (7/111)	0.911 (0.812–1.000)
Opposed-phase signal drop	0% (0/37)	30.6% (34/111)	0% (0/37)	32.4% (36/111)	0.963 (0.911–1.000)
LI-RADS category on CT (LR-3:4:5:M)	1:7:3:26	1:4:8:24	6:4:89:12	6:8:86:11	0.761 (0.662–0.859)
LI-RADS category on MRI (LR-4:5:M)	0:7:30	4:92:15	1:7:29	3:95:13	0.776 (0.673–0.878)

Note.—CT = computed tomography. MRI = magnetic resonance imaging. IMBCs = intrahepatic mass-forming biliary carcinoma. HCC = hepatocellular carcinoma. APHE = arterial phase hyperenhancement. DWI = diffusion-weighted image. LI-RADS = liver reporting and data system

Categorical variables are expressed as percentage with numerators and denominators or ratios. Kappa values are presented with the 95% confidence interval in parentheses

Figure 1

Study 1: Training set (Hospital A)



Study 2: Validation set (Hospital B)

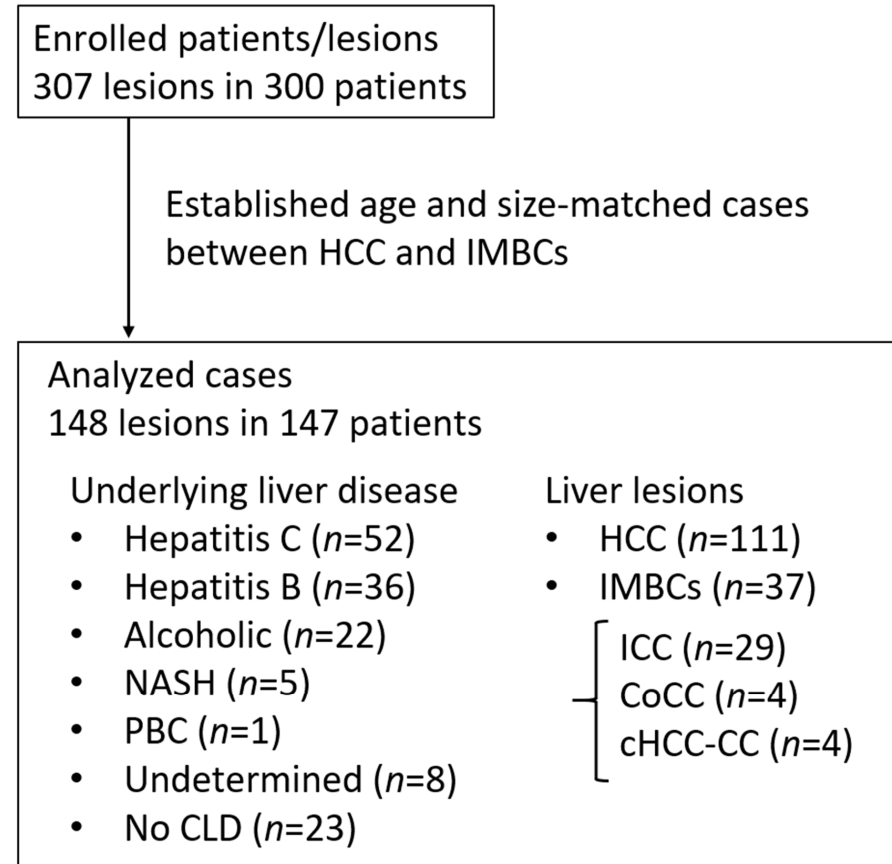
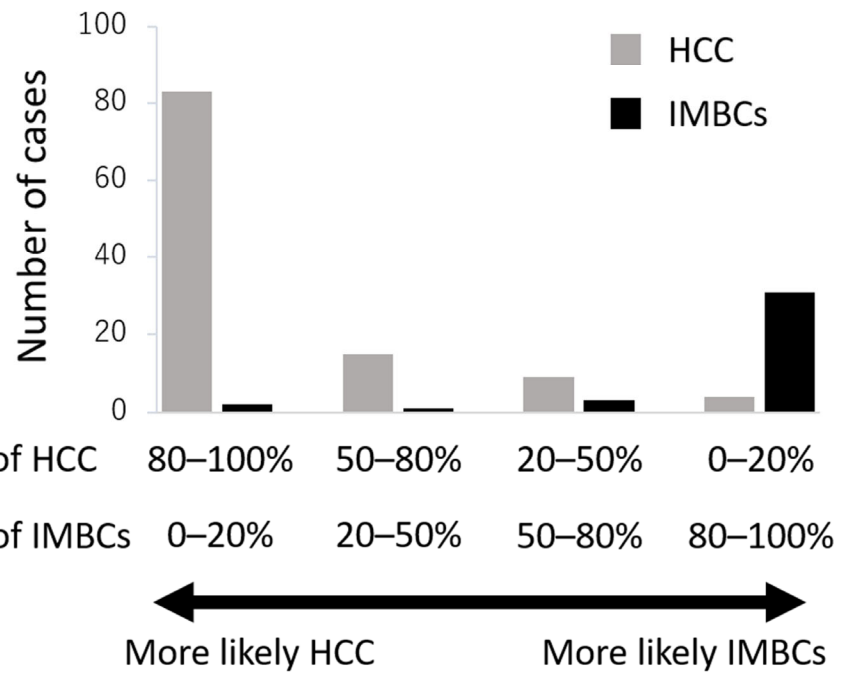


Figure 2

Reader 1



Reader 2

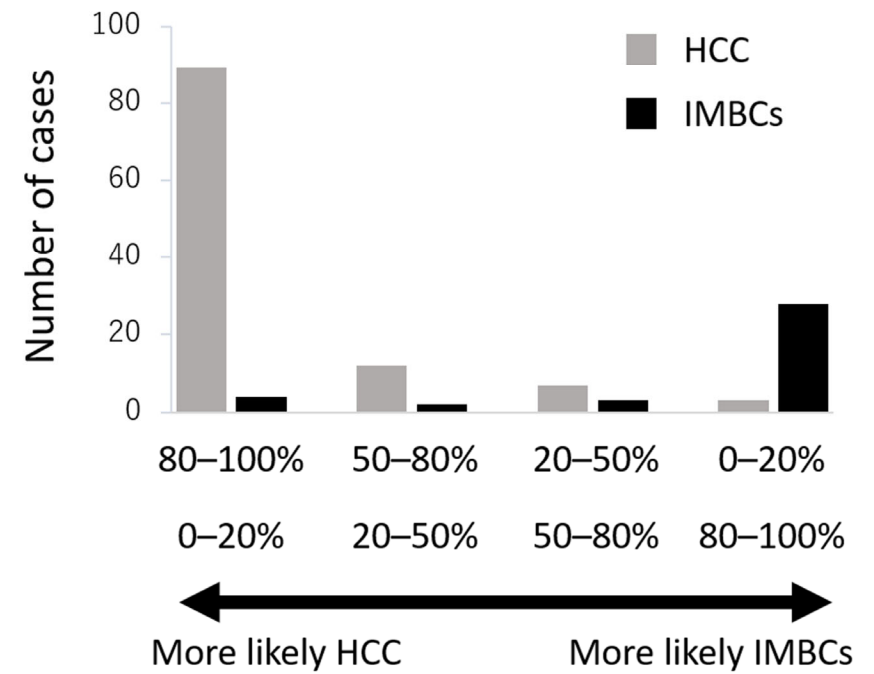


Figure 3

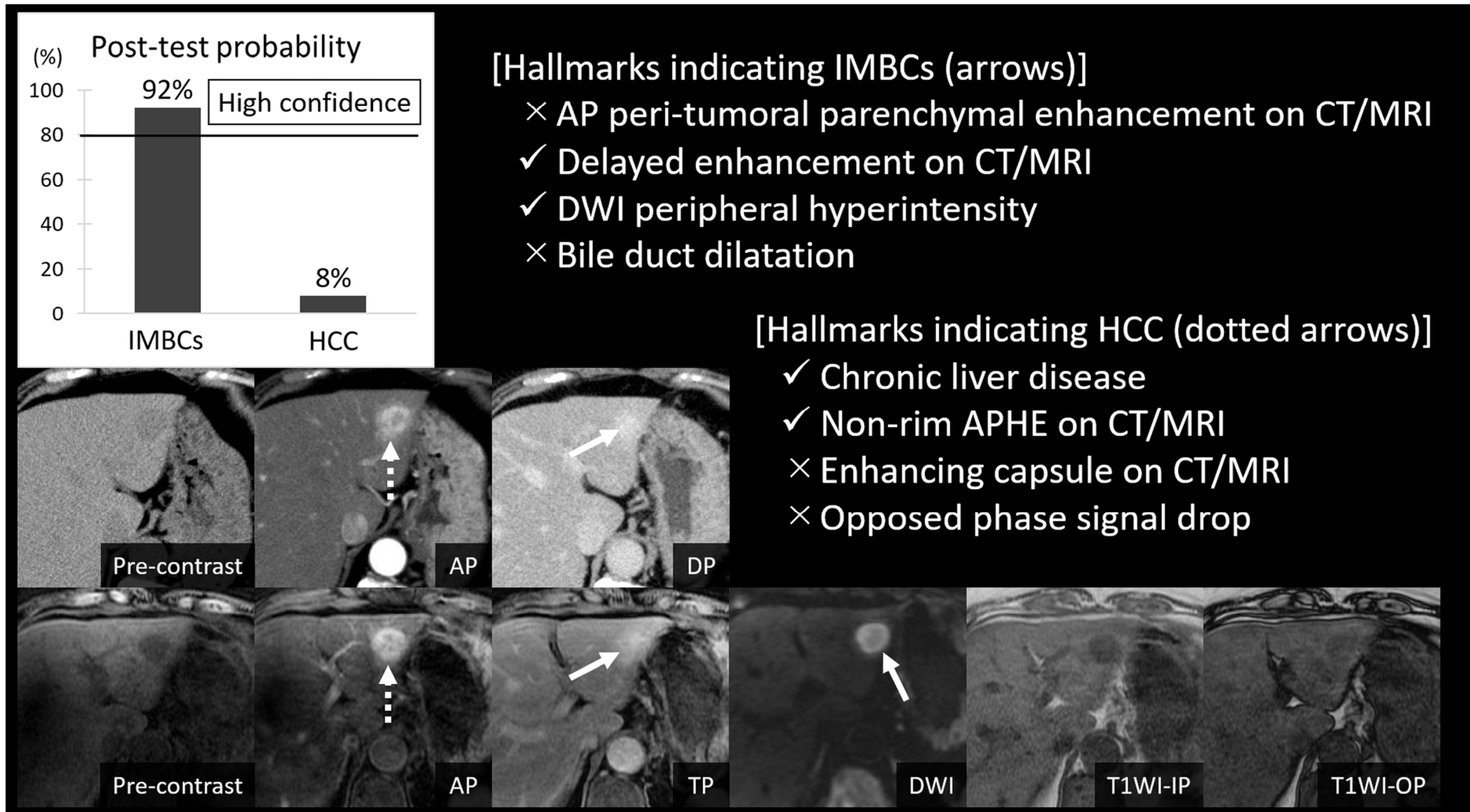


Figure 4

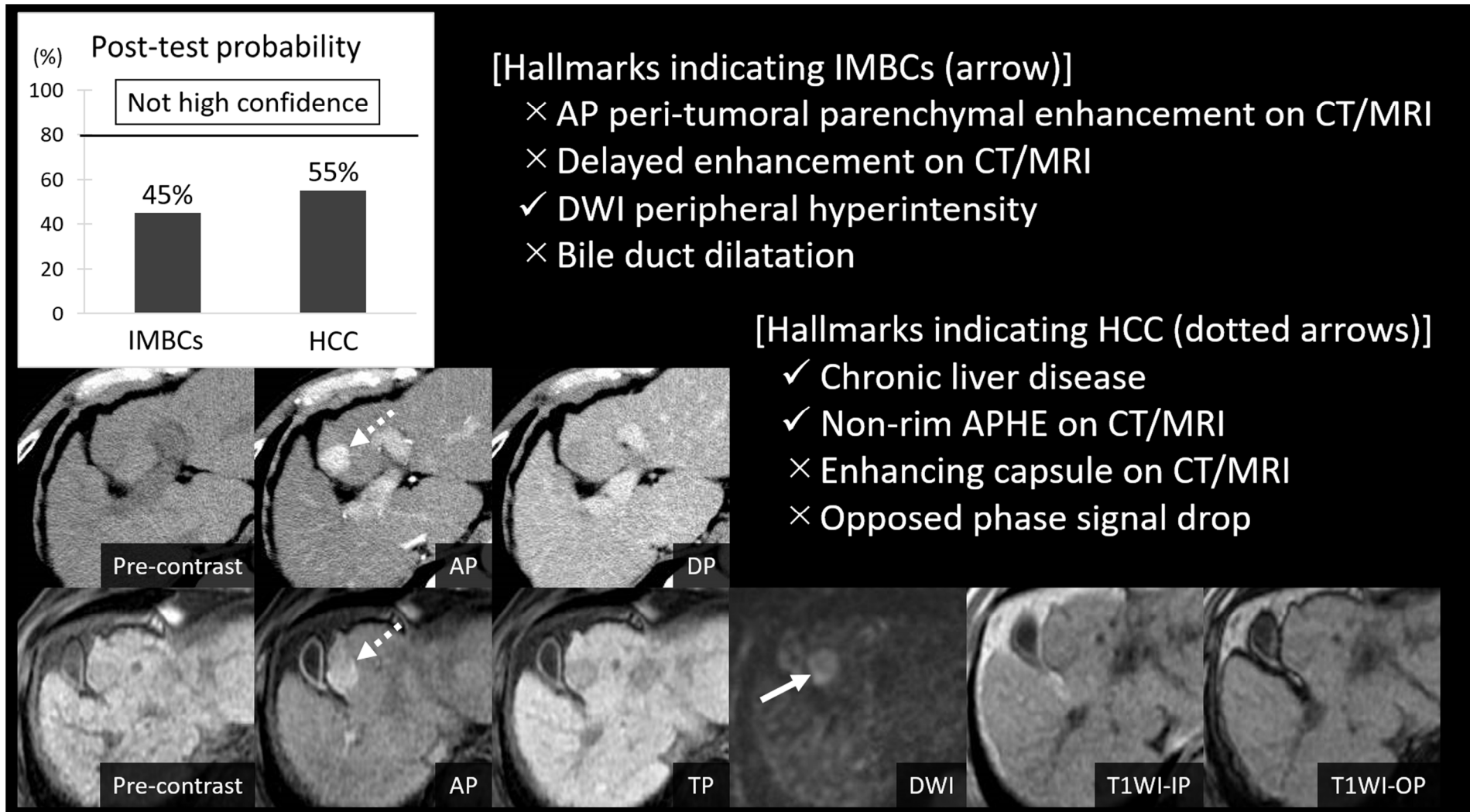


Figure 5

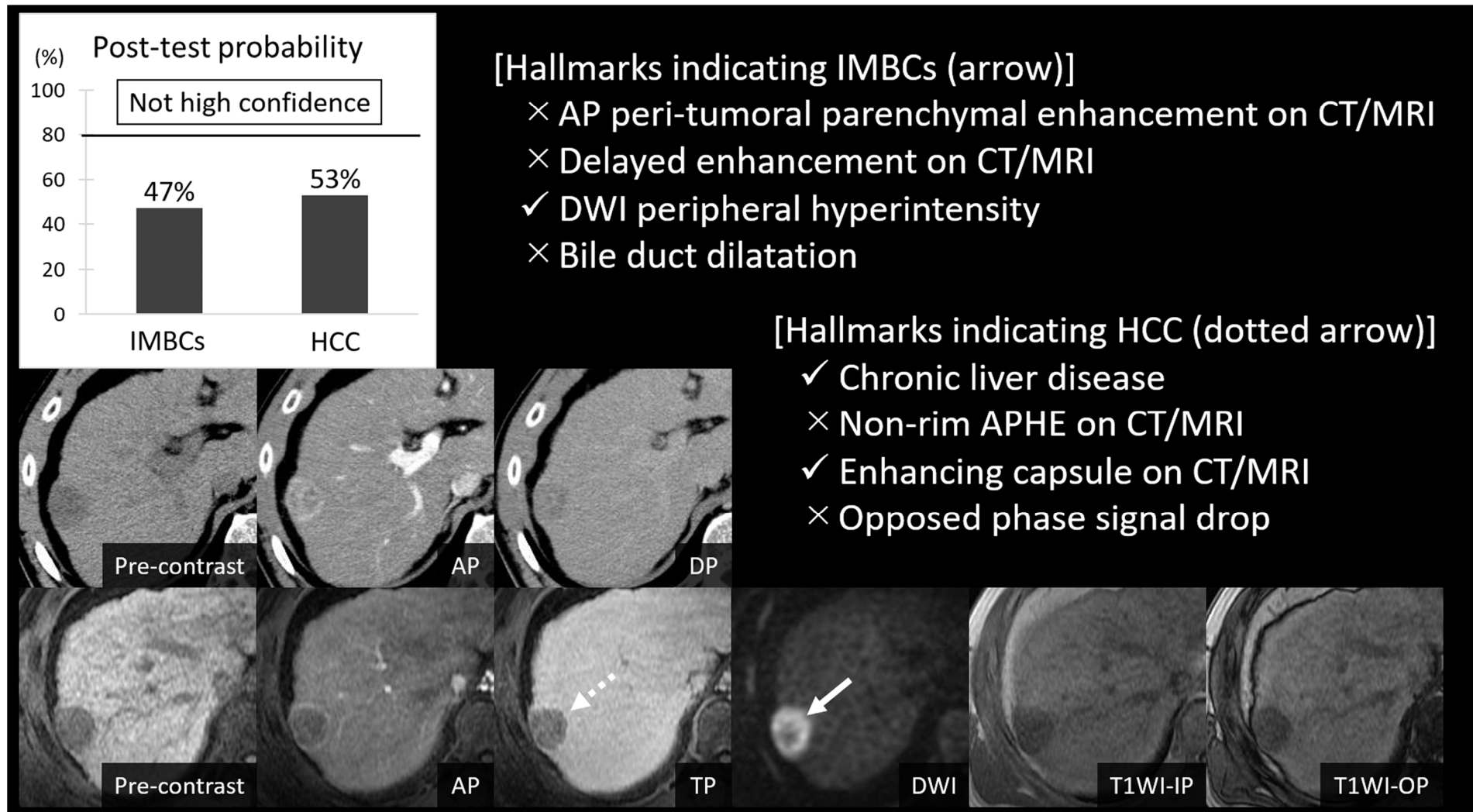
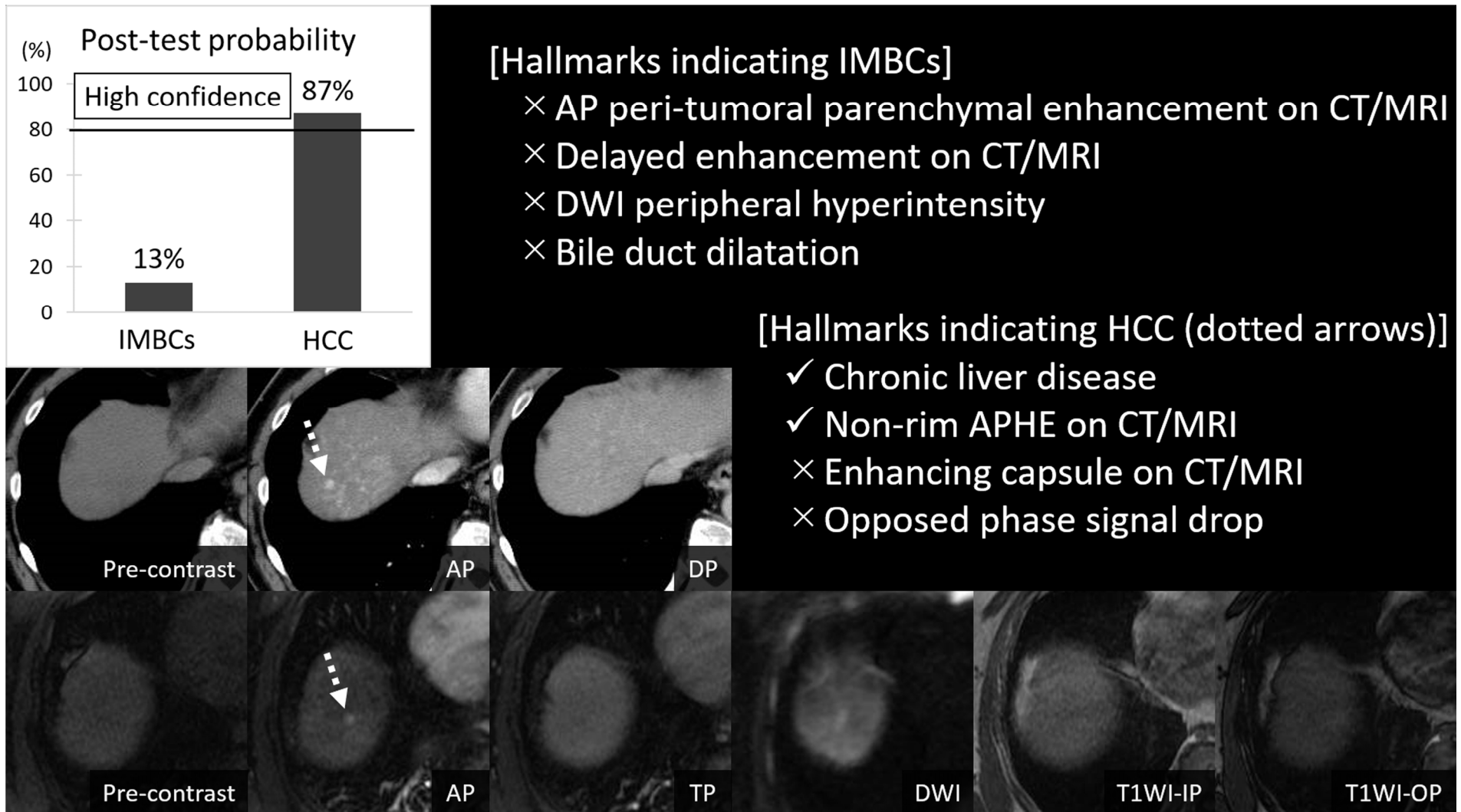


Figure 6



Supplemental Material 1. Parameters of CT

	Study 1	Study 2
CT machines	64- or 320-detector row units (Aquilion 64 or Aquilion ONE; Canon Medical Systems)	80 or 320-detector row units (Aquilion PRIME or Aquilion ONE; Canon Medical Systems)
Rotation time [s]	0.5	0.5
Beam collimation [mm]	64 × 0.5	80 × 0.5
Section thickness and intervals [mm]	5	5
Helical pitch (beam pitch)	0.828	0.813
Table movement [mm/s]	52.9	65.0
Scanning field of view [cm]	40	40
Voltage [kV]	120	120
Tube current [mA]	150–450	150–500
Effective mAs/slice	91–272	92–369

Note.—CT =computed tomography.

Supplemental Material 2. Parameters of MRI

	Study 1		Study 2	
MRI machines	1.5T (Signa EXCITE HD; GE Healthcare)	3T (Discovery 750; GE Healthcare)	1.5T (MAGNETOM Avanto; Siemens Healthineers)	3T (MAGNETOM Skyra; Siemens Healthineers)
T2-weighted image				
Sequence	Fat-saturated FSE	Fat-saturated FSE	Fat-saturated TSE	Fat-saturated TSE
Repetition time/echo time [ms]	2500–8000/64	3000–15000/78.5	2000–10000/81.0	2200–10000/85.0
Parallel imaging factor	1.75	2.0	1.0	3.0
Matrix	256 × 192	352 × 352	256 × 256	256 × 256
Field of view [cm]	32–40 × 32–40	32–40 × 32–40	32–40 × 32–40	35–40 × 35–40
Section thickness/intersection gap [mm]	6/0	5/1	6/1	5/1
Number of excitations	1	2	1	1
Flip angle [degree]	90	90	90	90
T1-weighted gradient-echo image				
Sequence	2D-fast GRE	3D-fast GRE	2D-fast GRE	2D-fast GRE

Repetition time/echo time [ms]	150–170/2.2 and 4.5	6.2/2.1 and 4.2	185/2.4 and 4.8	165/1.2 and 2.5
Parallel imaging factor	2	2	2	2
Matrix	32–40 × 32–40	35 × 16	256 × 158	256 × 186
Field of view [cm]	38 × 34.2	34 × 34	32–40 × 26–33	35–40 × 26–30
Section thickness/intersection gap [mm]	5/0	3.6/-1.8 (overlap)	6/1	4/1
Number of excitations	1	1	1	1
Flip angle [degree]	90	15	80	70

Diffusion-weighted image

Sequence	Single-shot SE-EPI	Single-shot SE-EPI	Single-shot SE-EPI	Single-shot SE-EPI
Repetition time/echo time [ms]	8000–10000/73	3000–10000/70	2000–10000/73	2000–10000/65
Parallel imaging factor	2	2	2	2
Matrix	128 × 128	128 × 192	128 × 78	128 × 86
Field of view [cm]	40 × 40	36 × 36	32–40 × 26–33	35–40 × 30–34
Section thickness/intersection gap [mm]	4–6/0–1	5/0	6/1	5/1
Number of excitations	4	8	4	4
Flip angle [degree]	90	90	90	90

b-value [s/mm ²]	0, 500, 1000	0, 500, 1000	0, 500, 1000	0, 500, 1000
Motion-proving gradients	3 axes (x (RL), y (AP), and z (SI))	3 axes (x (RL), y (AP), and z (SI))	3 axes (x (RL), y (AP), and z (SI))	3 axes (x (RL), y (AP), and z (SI))

Contrast-enhanced MRI

Sequence	3D-GRE T1WI (LAVA)	3D-GRE T1WI (LAVA)	3D-GRE T1WI (VIBE)	3D-GRE T1WI (VIBE)
Repetition time/echo time [ms]	3.8/1.9	4.8/2.0	3.3/1.3	2.8/1.1
Parallel imaging factor	1.75	2	1	2
Matrix	320 × 192	320 × 192	320 × 160	288 × 160
Field of view [cm]	35–42 × 40–45	34 × 27.2	32–40 × 24–30	35–40 × 26–30
Section thickness/intersection gap [mm]	5/-2.5 (overlap)	3.6/-1.8 (overlap)	5/0	3/0
Number of excitations	1	1	1	1
Flip angle [degree]	12	12	15	10
Scan delay after injection	Pre-contrast, 20–30 s, 1, 2, 20 min			

Note.—MRI = magnetic resonance imaging. FSE = fast spin echo. TSE = turbo spin echo. 2D = 2-dimensional. 3D = 3-dimensional. GRE = gradient echo. SE = spin echo. EPI = echo-planar imaging. RL = right-left. AP = anterior-posterior. SI = superior-inferior. T1WI = T1-weighted imaging. LAVA = liver acquisition with volume acceleration. VIBE = volumetric interpolated breath-hold examination.

Supplemental Material 3. Bayesian method for calculating post-test probability

A simple Bayesian classifier based on Bayes' theorem was adopted to make a diagnosis of HCC or IMBCs. The conditional probabilities of the classes were estimated by applying Bayes' rule using the statistical datasets of features, which were observed in clinical examinations as follows:

$$P(C_k|H_1, \dots, H_n) = \frac{P(C_k)P(H_1, \dots, H_n|C_k)}{P(H_1, \dots, H_n)},$$

where C_k ($k=1, 2$) is a possible class of HCC and IMBCs, and H_i ($i=1, 2, 3, 4$) denotes each observed feature. With the assumption of the independence of each factor, this formulation can be expressed as follows:

$$P(C_k|H_1, \dots, H_n) = P(C_k) \prod_{i=1}^{n=4} P(H_i|C_k)$$

The likelihoods $P(H_i|C_k)$ were calculated from the datasets of Study 2. We assumed the two prior possibilities were equiprobable. Therefore, the classification can be implemented by choosing the class with the highest post-test probability as the following equation:

$$k_c = \operatorname{argmax}_{k \in \{1,2\}} \prod_{i=1}^{n=4} P(H_i|C_k),$$

where k_c denotes the estimated result of the classification.